Journal of Nuclear Materials 406 (2010) 68–72

Contents lists available at ScienceDirect

Journal of Nuclear Materials

journal homepage: www.elsevier.com/locate/jnucmat

Calculation of phase diagrams and simulation of segregation using Monte Carlo with lattice relaxation

R. Anders *, F. Haider

Institut für Physik, Universität Augsburg, Universitätsstraße 1, 86159 Augsburg, Germany

A B S T R A C T

In order to model solids with strong internal elastic deformations a combination of Monte Carlo (MC) and lattice relaxation was developed. Using this method the phase diagrams corresponding to EAM potentials for Fe–Ni and Fe–Cu were determined and segregation to an edge dislocation and a grain boundary were simulated. In the case of the dislocation the resulting critical shear stress was calculated.

1. Introduction

The simulation of segregation or phase separation is a difficult task, since the relevant mechanisms take place on different time scales. Diffusion usually takes hours or days, while the elastic lattice deformation due to atomic rearrangements happens within nanoseconds.

To overcome this problem different methods have been proposed in the literature, which use a combination of MC and lattice relaxation. A method developed by Fratzl and Penrose [1,2] is based on an Ising model. It uses harmonic interatomic forces, which allows for a very efficient treatment of elastic deformations. However, strong deformations, which are present near dislocations or in alloys with large size misfit, are not well approximated by harmonic forces.

Another method, proposed by Finel [3], uses two different types of MC steps, namely an exchange between neighbouring atoms or an atomic displacement. Thus not only configurational but also vibrational entropy is taken into account, and lattice relaxation is incorporated in an elegant way. A drawback, however, is that atomic exchanges may be performed before the elastic energy is completely minimised.

Our approach is to perform a lattice relaxation after each MC step to ensure that the elastic energy is minimal before attempting the next step. Since a relaxation of the complete lattice would be too time-consuming we chose an algorithm that does only local modifications in the MC step. Thus we can confine the relaxation to a few atoms in the vicinity of the modification.

2. Simulation method

The simulations described here were carried out using a Metropolis MC algorithm on systems with fixed temperature and total number of atoms but variable composition. The atomic interactions were calculated with the embedded-atom method (EAM) [4].

In each MC step the type of a randomly chosen atom is changed and the resulting difference $\Delta\widetilde{E}$ in potential energy is calculated. The change of type can be thought of as a two-step process: First an atom is removed from the system and put into a reservoir of chemical potential μ_{old}. Afterwards an atom from a different reservoir (chemical potential μ_{new}) is put into the system at the same position. Hence the total difference in energy is $\Delta E = \Delta\widetilde{E} + \mu_{\text{old}} - \mu_{\text{new}}$. In the case of a binary alloy the difference $\mu_{\text{old}} - \mu_{\text{new}}$ can only take one of the two values $\pm\Delta\mu$, where $\Delta\mu$ is the difference in chemical potential for the two atom types.

If the energy difference $\Delta E = \Delta\widetilde{E} \pm \Delta\mu$ is positive (increase), the type flip is rejected with a probability of $1 - \exp(-\Delta E/(k_B T))$, otherwise it is accepted. The loop terminates if the relative change in the concentration (averaged over a certain amount of steps) falls below a given limit. Thus the composition of the system approaches its equilibrium value, which depends on the given parameters $\Delta\mu$ and T (temperature).

For each direction in space the boundaries of the simulation cell can either be treated as free surfaces, or fixed periodic boundary conditions (PBC) can be applied. If PBC are used for all directions this results in a constant volume simulation ($TV\Delta\mu$-or semi-grand canonical ensemble). If all surfaces are free, the ensemble is $Tp\Delta\mu$ with $p = 0$.

The main loop of the program consists of the MC step and a lattice relaxation around the modification ("local relaxation", within a radius of ≈6 Å). In the beginning and every 10,000 MC steps a relaxation of the complete lattice ("global relaxation") is performed in

* Corresponding author.
E-mail address: rolf.anders@physik.uni-augsburg.de (R. Anders).

0022-3115/$ - see front matter © 2010 Elsevier B.V. All rights reserved.
doi:10.1016/j.jnucmat.2010.07.048

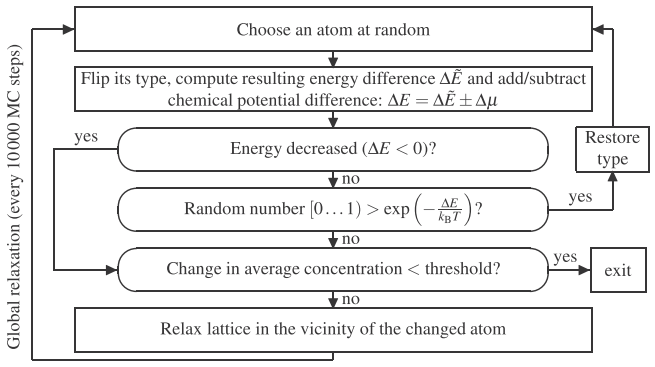

Fig. 1. MC algorithm with relaxation.

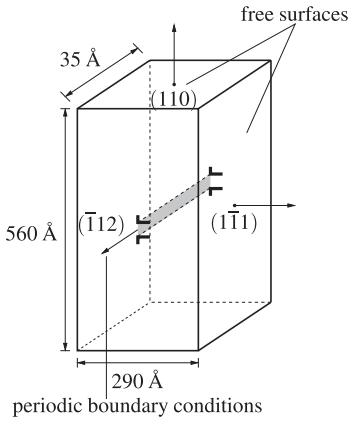

Fig. 2. Geometry of the simulation cell.

order to prevent the system to deviate too far from equilibrium (Fig. 1).

The relaxation is based on the Gear predictor–corrector algorithm (see e.g. [5]), which is frequently used in molecular dynamics (MD), and works as follows: First the atomic positions, velocities and some higher order derivatives are predicted for the next time step based on the current values using a Taylor expansion. Then the forces and their deviations from the predicted values are calculated (forces and accelerations are made equal by setting the masses to unity). In the next step a correction term, which is proportional to the force deviation, is added to the predicted quantities. This procedure is repeated until the energy increases. Then the last step is taken back, the kinetic energy is removed by setting the velocities to zero and the loop is restarted with a smaller time step. The algorithm terminates when the maximum force falls below a given limit.

3. Results

3.1. Segregation to an edge dislocation

The stress field of an edge dislocation contains (besides shear components) regions with positive and negative pressure. Hence in an alloy with size misfit one expects the larger atoms to accumulate in the dilatation region and to deplete in the compression region. The inhomogeneous distribution of solute atoms around the dislocation lowers its energy and therefore increases the force needed to move it, which results in a higher yield stress of the material.

As an alloy with high size misfit, Ni–Al [6,7] was used (lattice constants: a_{Ni} = 3.52 Å, a_{Al} = 4.05 Å). The fitting procedure for this potential was aimed essentially at a good agreement of the elastic constants of Ni, Al and $L1_2$–Ni_3Al with experimental values, while reproducing the lattice constants and cohesive energies exactly. Since the size misfit is large, the elastic properties of the material play a major role for segregation. Hence this potential is assumed to be suitable here, although segregation energies were not considered in the fit.

The simulation was started with pure Ni (516,096 atoms) with an edge dislocation at the center of the cell, which splits into two partials during the initial relaxation. Due to the underestimation of the stacking fault energy by the potential the separation is relatively large (20*b* instead of 4*b* [8], *b*: length of the Burgers vector). Periodic boundary conditions were applied along the dislocation line (Fig. 2). In order to obtain a sharp concentration profile, a rather low temperature of *T* = 300 K was used. The chemical potential difference $\Delta\mu$ was chosen to yield an equilibrium Al concentration of v_{Al} = 0.034, which was reached after 2,000,000 MC steps.

The regions of highest compression of the two partial dislocations have significantly decreased Al concentration, but are hardly visible in the simulation cell (Fig. 3, above and below the center). The Al depletion and enrichment can be seen quantitatively in the concentration profile which refers to a slice (between the two planes in Fig. 3) containing only the lower partial dislocation. Here the depletion is visible mainly in the first two $(1\bar{1}1)$-layers to the right of the slip plane.

In order to determine the critical shear stress τ_c of the material, the resulting atomic configuration was exposed to external shear stress in a molecular dynamics simulation using xmd [9]. The shear stress was generated by applying an external force in $[1\bar{1}0]$-direction to each atom on the $(1\bar{1}1)$-surface and an opposite force on the opposite surface. In order to compensate the resulting torque,

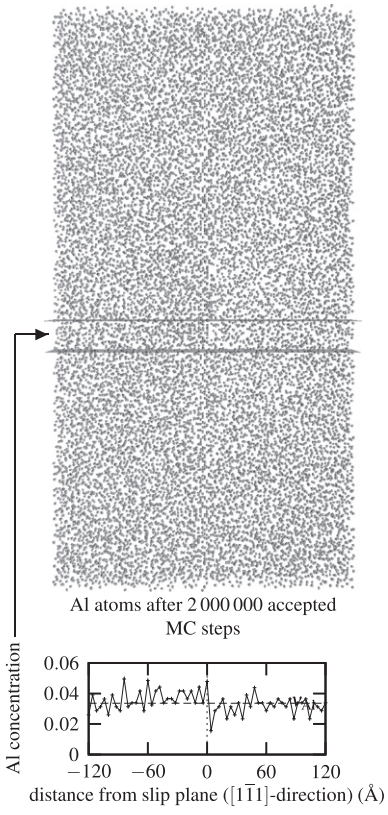

Fig. 3. Projection of the Al distribution onto the $(1\bar{1}2)$-plane and concentration profile for the slice containing the lower partial dislocation; the average concentration is indicated by the dashed line. The orientation of the simulation cell is the same as in Fig. 2, i.e. the dilatation region is on the left of the slip plane and the compression region on the right.

an appropriate force in $\pm[1\bar{1}1]$-direction was applied to the atoms on the $\pm(1\bar{1}0)$-surface respectively.

The MD simulation was run with a time step of 2 fs. During the first 10,000 MD steps the system was relaxed by setting the velocities of all atoms to 0 every 250 steps. In the following 500 steps xmd's quench algorithm was applied, which is like regular MD, but stops all atoms whenever the potential energy is higher than in the previous step. Afterwards regular MD was used and the shear stress was increased in steps of 20 MPa every 500 MD steps. No temperature control was applied in the MD simulation to avoid a time-consuming warm-up phase. The temperature stayed below 0.1 K after quenching.

In Fig. 4 the positions of the two partial dislocations are plotted against the applied shear stress at the beginning of each phase of constant load. The positions were determined by filtering out the 100 atoms with highest potential energy, assigning each one to a dislocation and separately averaging over their coordinates. Both dislocations remain at their initial positions up to 80 MPa and start moving at 100 MPa, which yields a critical shear stress of $\tau_c = (90 \pm 10)$ MPa.

In order to estimate the influence of segregation an equivalent MD simulation with pure Ni was carried out. It was started with the same initial atomic positions and an increment of 0.5 MPa in shear stress. In this simulation the critical shear stress cannot be accurately determined since the dislocations already move at very low stresses and partly in the wrong direction (Fig. 5). The reason for this behaviour probably lies in the interaction between the dislocations, which might not have had their exact equilibrium distance in the beginning. From Fig. 5 the critical shear stress can be estimated as approximately 10 MPa, which lies in the same order of magnitude as the experimental value 580 p/mm^2 (=5.69 MPa) given by Böhm [10] for Ni of 99.8% purity. In spite of the inaccuracy it is clear, that the critical shear stress is greatly enhanced by the solute Al atoms.

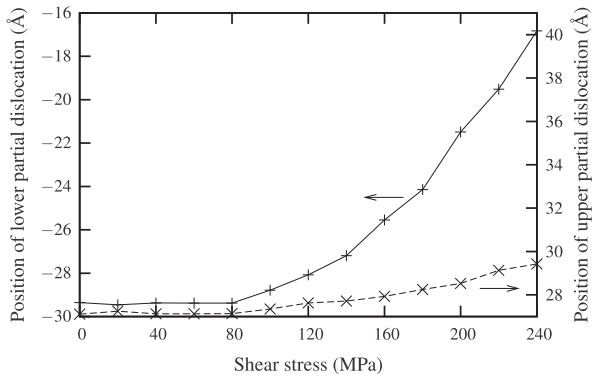

Fig. 4. Positions of the partial dislocations during MD simulation of Ni–Al.

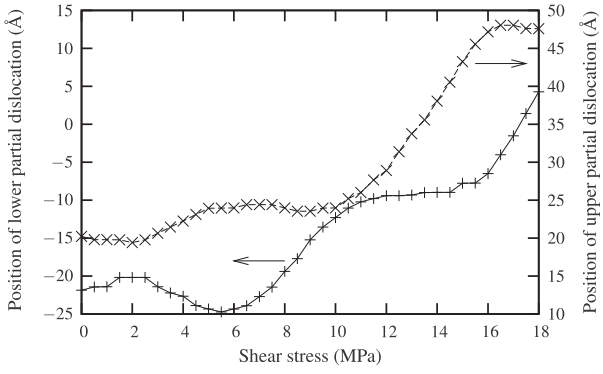

Fig. 5. Positions of the partial dislocations during MD simulation of pure Ni.

3.2. Calculation of phase diagrams

Simulations with direct manipulation of atom types lead to thermodynamic equilibrium quite rapidly since atomic transport takes place without diffusion. Hence they can be used to efficiently determine the phase diagram of a material defined by a given potential: Simulations at different temperatures and chemical potential differences $\Delta\mu$ are run and the resulting structures are analysed.

This procedure was applied to the Fe–Ni and Fe–Cu systems using EAM potentials from Bonny et al. ([11,12] and references therein). A simulation cell of 4032 atoms was used in both cases, with free surfaces in the case of Fe–Ni. Periodic boundary conditions had to be used for Fe–Cu, since otherwise significant surface segregation was observed.

At each temperature T a series of simulations with monotonically changing $\Delta\mu$ was carried out. For subsequent simulations within a series the equilibrium configuration of the previous one was used as the starting point. For each system this procedure was run twice, once for increasing $\Delta\mu$ and once for decreasing $\Delta\mu$, i.e. starting at different sides of the phase diagram. For Fe–Ni the calculation starting with pure Ni was done in two variants: once with relaxation (as for Fe–Cu) and once without relaxation except for the initial one at each T and $\Delta\mu$.

The Fe–Cu potential was made primarily for the simulation of irradiation damage. Hence the focus was put onto defect binding energies, but the solubility of Cu in Fe is also reproduced quite well. The aim for the Fe–Ni potential was to reproduce the phase diagram in the whole concentration range. Therefore the mixing enthalpy was considered in the fit and constraints were applied to ensure that $L1_0$ and $L1_2$ are the only ground states of the mixture. Thus it is expected that both potentials show phase diagrams which are close to the experimental ones.

In the Fe–Ni system four stable phases were found (Figs. 6 and 7), whereas the ordered fcc phases are only observed at temperatures below 1900 K (1700 K without relaxation). Analysis of the resulting structures identifies these as bcc Fe, $L1_0$, $L1_2$ and fcc Ni. These phases were also observed experimentally [13]. However, $L1_0$ Fe–Ni is probably metastable and the $L1_2$ phase is only stable below 790 K. Considering that both Fe and Ni are ferromagnetic elements, it is not surprising that the experimental phase diagram is not reproduced more closely, since magnetic interaction can only be treated in an effective way by an EAM potential [14] and was not taken into account by the potential used in this calculation.

The phase diagram obtained from simulations without relaxations (except for the global one at the beginning) is drawn as

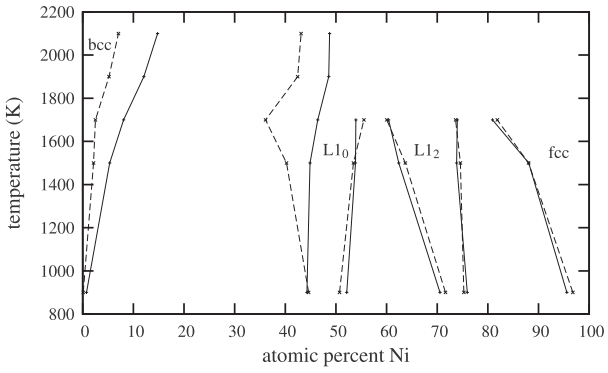

Fig. 6. Fe–Ni phase diagram, starting with pure Ni (with relaxation: —-, only initial relaxation: - - -).

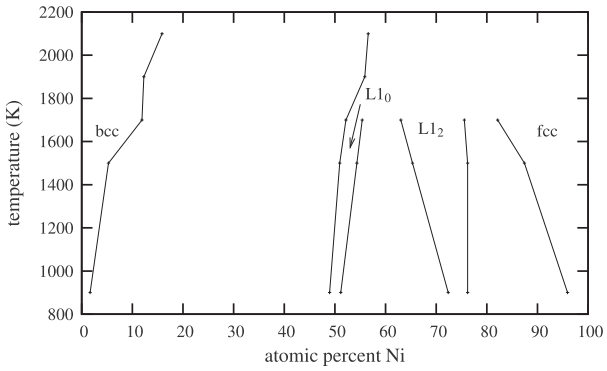

Fig. 7. Fe–Ni phase diagram, starting with pure Fe.

dashed lines for comparison. Transitions between the fcc phases occur at roughly the same concentrations in both cases, whereas the fcc–bcc transformation is shifted to lower concentrations. This observation demonstrates the importance of relaxations for phase transitions with structural changes.

A phase diagram was also calculated by the authors of the potential [11], who used the Alloy Theoretic Automated Toolkit (ATAT) [15]. The calculation was done in two variants, with and without accounting for vibrational entropy, the latter one being comparable to our method. The Fe–Ni phase diagrams presented here are essentially similar to the one calculated with ATAT ignoring vibrational entropy: The same phases were found and reside in similar regions of concentration and temperature.

Figs. 8 and 9 show the calculated phase diagram for Fe–Cu. The large miscibility gap is in accordance with the experimental phase diagram [13]. However, the solubility of Fe in Cu is somewhat

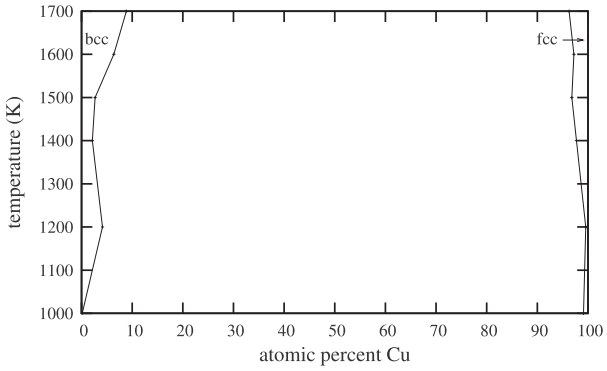

Fig. 8. Fe–Cu phase diagram, starting with pure Cu.

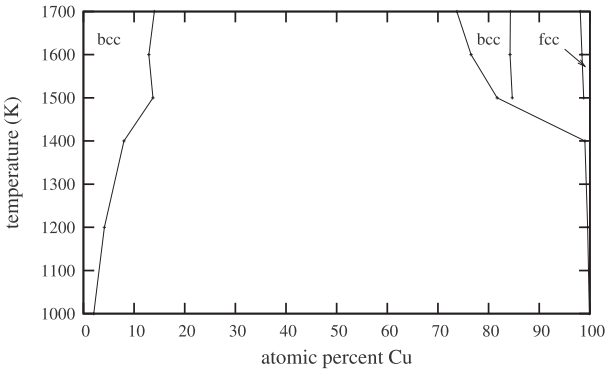

Fig. 9. Fe–Cu phase diagram, starting with pure Fe.

lower in the simulation. The reason probably lies in the use of fixed periodic boundary conditions, which were applied to prevent surface segregation. The constant volume and shape of the simulation cell can lead to significant stress, thus lowering the solubility.

In the phase diagram where the calculations start with pure Fe (Fig. 9) a Cu-rich bcc phase appears at temperatures above 1500 K. Similarly a bcc phase which even extends over the whole concentration range at temperatures near 1600 K was found by Lopasso et al. [16] in the Fe–Cu system with a different EAM potential.

The concentration dependence of the stability of Fe–Cu alloys using ab initio and cluster expansion techniques was investigated by Liu et al. [17]. By calculating different elastic properties they found that the bcc phase is elastically stable up to Cu concentrations around 50% and that the stability is enhanced by an Fe matrix for Cu-rich precipitates. This observation is consistent with measurements of the concentration in small Cu-rich precipitates in Fe, which are summarized in the same paper.

However, since the Cu-rich bcc phase in our simulation is not ordered and does not occur if the calculations start with pure Cu, it is likely that the simulation did not reach equilibrium in this case. I.e., the structural transformation did not happen due to limited computing time.

3.3. Segregation to grain boundaries

Experimentally the solute concentration on grain boundaries is usually measured using Auger electron spectroscopy on surfaces of samples fractured under ultra-high vacuum. This may not give representative results, since the probability for a crack at a certain

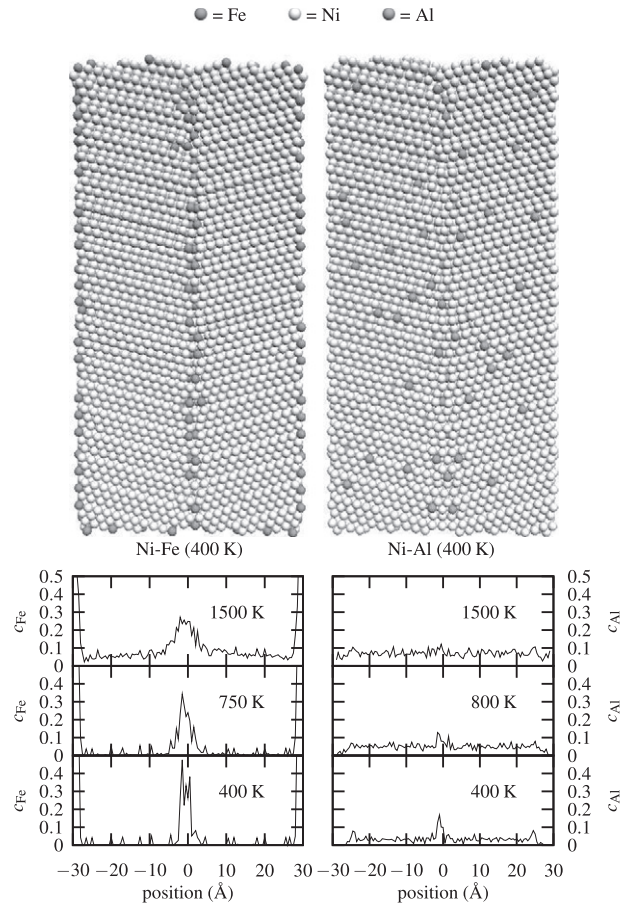

Fig. 10. Grain boundary segregation: Simulation cells and concentration profiles after 400,000 MC steps ($(1\bar{1}2)$-cut).

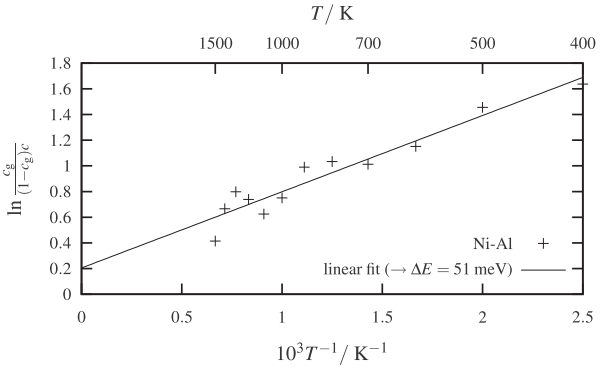

Fig. 11. Langmuir–McLean plot for Ni–Al.

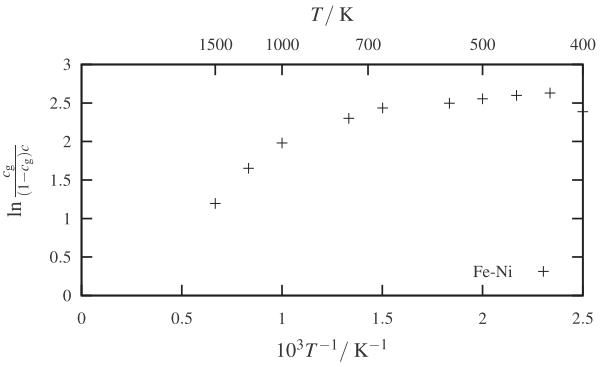

Fig. 12. Langmuir–McLean plot for Ni–Fe.

grain boundary depends on its enrichment factor, i.e., the ratio of its concentration to the bulk concentration. Simulations can give an indication of the reliability of this experimental method, because here the enrichment can be determined independently of the crack probability.

A theory that describes the temperature dependence of segregation to grain boundaries was proposed by McLean [18]. In this theory lattice sites are divided into two types, grain boundary and bulk, with potential energies e and E respectively. The equilibrium distribution of solute atoms is then determined by the minimum of the free energy F. For dilute systems (bulk concentration $c \ll 1$) this leads to the following relation between grain boundary concentration c_g and temperature T:

$$\frac{E-e}{k_B T} = \ln \frac{c_g}{(1-c_g)c} \tag{1}$$

Hence, a plot of $\ln \frac{c_g}{(1-c_g)c}$ over $1/T$ should give a linear relation with slope $(E-e)/k_B$.

Corresponding diagrams from simulations of Ni–Fe [19] and Ni–Al [6,7] are shown in Figs. 11 and 12. The simulation cells consisted of 44,160 atoms each and were prepared with a 30° tilt grain boundary. Periodic boundary conditions were used along the tilt axis ($[1\bar{1}2]$) (Fig. 10). The grain boundary was constructed by cutting a single crystal into halves, rotating them by ±15° respectively, cutting the tilted surfaces horizontally and vertically, putting the halves together and relaxing the lattice.

In the Ni–Al system the linear relation (1) is fulfilled quite well. A linear fit yields an energy difference of 51 meV. For Ni–Fe, however, the low temperature data points deviate strongly from the linear behaviour. The reason lies in the rather high grain boundary concentrations, which are reached especially at low temperatures. This strong enrichment leads to significant interaction between solute atoms, hence the assumption of a constant energy for grain boundary sites is no longer valid.

4. Conclusion

The combination of MC with lattice relaxation can be used to simulate many different phenomena which are relevant for the mechanical characteristics of alloys. The calculation of phase diagrams can show which phases are described well by the potential and contribute to the optimisation of potentials. Segregation to grain boundaries can strongly influence the brittleness of a material and is difficult to measure experimentally. Similarly the segregation to dislocations affects the critical shear stress. Thus simulations can help to analyse the microstructure and its effect on mechanical properties.

Acknowledgements

This work was supported through the integrated project PERFECT of the 6th Framework Programme of the European Commission under Contract Number FI6O-CT-2003-508840. R. Anders likes to thank G. Bonny from SCK·CEN for providing the Fe–Cu–Ni EAM potential and C. Müller for taking the time for various helpful discussions.

References

[1] P. Fratzl, O. Penrose, Acta Metallurgica et Materialia 43 (8) (1995) 2921–2930.
[2] C.A. Laberge, P. Fratzl, J.L. Lebowitz, Acta Metallurgica et Materialia 45 (10) (1997) 3949–3961.
[3] A. Finel, Dynamics in elastically stressed alloys: growth laws in phase separating systems; Monte Carlo simulations, in: Phase Transformations and Evolution in Materials, 2000, pp. 371–385.
[4] M.S. Daw, M.I. Baskes, Physical Review Letters 50 (17) (1983) 1285–1288.
[5] M.P. Allen, D.J. Tildesley, Computer Simulation of Liquids, Oxford University Press, New York, 1991.
[6] A.F. Voter, S.P. Chen, Accurate interatomic potentials for Ni, Al and Ni_3Al, in: Materials Research Society Symposia Proceedings, vol. 82, 1987, pp. 175–180.
[7] A.F. Voter, The embedded-atom method, in: J.H. Westbrook, R.L. Fleischer (Eds.), Intermetallic Compounds: Principles and Practice, vol. 1, John Wiley & Sons, 1995 (pp. 77–90, Chapter 4).
[8] J.S. Koehler, Physical Review B 2 (2) (1970) 547–551.
[9] J. Rifkin, xmd, <http://xmd.sourceforge.net>.
[10] H. Böhm, Einführung in die Metallkunde, Bibliographisches Institut Wissenschaftsverlag, Mannheim, 1968.
[11] G. Bonny, R.C. Pasianot, L. Malerba, Modelling and Simulation in Materials Science and Engineering 17 (2009) 025010.
[12] R.C. Pasianot, L. Malerba, Journal of Nuclear Materials 360 (2007) 118–127.
[13] T.B. Massalski (Ed.), Binary Alloy Phase Diagrams, American Soc. for Metals, Metals Park, Ohio, 1987.
[14] S.L. Dudarev, P.M. Derlet, Journal of Physics: Condensed Matter 17 (2005) 7097–7118.
[15] A. van de Walle et al., Atat, <http://www.its.caltech.edu/avdw/atat/>.
[16] E.M. Lopasso, M. Caro, A. Caro, P.E.A. Turchi, Physical Review B 68 (21) (2003) 214205.
[17] J.Z. Liu, A. van de Walle, G. Ghosh, M. Asta, Physical Review B 72 (14) (2005) 144109.
[18] D. McLean, Grain Boundaries in Metals, Clarendon Press, Oxford, 1957.
[19] R.J. Meyer, Computersimulationen martensitischer Phasenübergänge in Eisen–Nickel- und Nickel–Aluminium-Legierungen, Ph.D. thesis, Universität-Gesamthochschule Duisburg, 1998.